Multiphase and Multi-component Interactions through the Unsaturated Saturated Zone Field and Model Study

S. Sorek[1, 2], M. Kuznetsov[1], A. Yakirevich[1], D. Ronen[1,3]

[1] Ben-Gurion University of the Negev, J. Blaustein Institutes for Desert Research, Zuckerberg Institute for Water Research, Environmental Hydrology & Microbiology, Sde Boker Campus, 84990, Israel
[2] Ben-Gurion University of the Negev, Mechanical Engineering, Pearlstone Center for Aeronautical Engineering Studies, Beer Sheva, 84105, Israel
[3] Water Quality Division, Israel Water Commission, POB 20365, Tel-Aviv, 61203, Israel

Corresponding author: Midreset Ben-Gurion, Sde Boker Campus 84990 Israel – Tel: +972 8 6596902 – Fax: +972 8 6596909 – e-mail: sorek@bgumail.bgu.ac.il

Abstract

An integrated approach of field and model investigations was implemented to an aquifer underlying urban infrastructure. The study focuses on the transport of Trichloroethylene (TCE) through the unsaturated-saturated zone. Simulations, subject to isothermal conditions, addressed a three-dimensional continuum involving three interacting mobile phases: aqueous, NAPL (Non-Aqueous Phase Liquids) and gaseous. The mathematical model considers water, air and TCE as components in equilibrium partitioning between the three mobile fluids, while for the latter we account also for sorption on the solid matrix. Predictions of migration patterns were due to a continuous spill from a single NAPL source situated at the soil surface.

The specific flux of the gaseous phase proved to be directed to the surface at the vicinity of impervious segments, implying that TCE vapors may surround building foundations. We note a vertical, gravity driven, NAPL

stem penetrating through the unsaturated-saturated zones. This causes a vertical displacement of the gaseous phase the velocity of which is also influenced by the gaseous pressure gradient. Fluids densities depend on TCE concentration, we thus note a density driven flow pattern. As TCE concentration decreases away from the NAPL stem, the gradient of the gas density yields its horizontal displacement, and vertical outward shift resulting from the vanishing capillary pressure. The gaseous velocity far away from the stem is associated only with the gas pressure gradient and is diminished at the unsaturated-saturated boundary, as the relative permeability of gaseous phase decreases near the capillary fringe.

Keywords

Multiphase; multi-component; urban; modeling

Introduction

The objective of the study was to examine by means of numerical simulations and available field observations, the temporal and spatial distribution of TCE resulting from leakage of NAPL at a prescribed location in the unsaturated and saturated zones of the Tel Aviv area. To achieve this goal, a three-dimensional (3-D) mathematical model of three ℓ phases and three p components *l(≡ n - NAPL, q - aquenous; g - gaseous)*, *p(≡ w water; a – air; c_m – contaminants)* was used. The flow and transport of this multiphase and multi-component problem is a coupled mechanism, as explained in the following. The *linear momentum balance equation (Darcy's law)* for each l phase reads

$$\mathbf{V}_l = -\mathbf{K}\frac{k_{rl}}{\mu_l}\left(\nabla P_l + \rho_l g \nabla Z\right), \quad \forall l \tag{1}$$

where $\mathbf{V}_l\,[m\,s^{-1}]$ denotes the l phase velocity vector, $\mathbf{K}[m^2]$ denotes the absolute permeability tensor, k_{rl} denotes the relative permeability of the l phase, $\mu_l[Pa\,s]$ denotes the l phase viscosity, $g[m\,s^{-2}]$ denotes the gravitational acceleration, $Z[m]$ denotes the altitude above some level and $\rho_l[kg\,m^{-3}]$ denotes the l phase mass density. The latter suggests a density driven flow as its *state function* is defined by

$$\rho_l = M_l \sum_p W_p X_{pl}; \qquad \sum_p X_{pl} = 1, \ \forall l, p \tag{2}$$

where $W_p[kg\ mole^{-1}]$ denotes the molecular weight of the p component, $M_l[mole\ m^{-3}]$ denotes the l phase molar density and X_{pl} denotes the mole fraction of the p component in the l phase. The *state functions* of X_{pl} are associated with $P_l[Pa]$ the l phase pressure, reading

$$X_{c_m g} = \frac{X^*_{c_m g} P^*_g}{P_g} X_{c_m n}; \quad X_{c_m g} = \frac{X^*_{c_m g} P^*_g}{X^*_{c_m q} P_g} X_{c_m q}; \quad X_{wg} = \frac{\beta_{wgq}}{P_g} X_{wq}$$
$$M_g = \frac{P_g}{RT^*}; \quad M_l \Big/ M^*_l = 1 + \chi_l \left(P_l - P^*_l \right), \quad l \equiv q,n \tag{3}$$

in which $P^*_l[Pa]$ denotes the l phase reference pressure, $X^*_{c_m l}$ denotes the mole fraction of TCE in equilibrium with the $l \equiv g,q$ phases and $\beta_{wgq}[Pa]$ denotes the partial pressure of the water component in the gaseous phase which is in equilibrium with the aqueous phase, M^*_l denotes the l phase molar density at the P^*_l pressure, $R[Pa\ m^3\ mole^{-1}\ ^\circ K]$ denotes the ideal gas constant and $T^*[^\circ K]$ denotes a reference temperature and $\chi_l[Pa^{-1}]$ denotes the l phase pressure compressibility. The phase pressures are related through the capillary pressures $(P_{c l_1 l_2})$ in the form

$$P_g = P_n + \alpha P_{c\,gn}(S_g) + \left(1 - \alpha\right)\left[P_{c\,gq}(S_g) - P_{c\,nq}(S_q = 1) \right]; \qquad \sum_l S_l = 1, \ \forall l;$$
$$P_n = P_q + \alpha P_{c\,nq}(S_q) + \left(1 - \alpha\right) P_{c\,nq}(S_q = 1) \tag{4}$$

where S_l denotes the saturation of the l phase, $\alpha = \min\left(1, S_n \big/ S^*_n\right)$ and S^*_n denotes a blending parameter associated with the NAPL phase.

Simulations were performed with the COMPFLOW code (Unger et al. 1996).

The actual contamination problem was solved over a total area of about 65.6 km2. The study area is part of the Coastal Plain aquifer of Israel which is mainly composed of layers of Pleistocene sand, sandstone and silt with intercalations of clay and loam. Some of the intercalations are discontinuous lenses; others near the coast are continuous and separate the aquifer into sub-aquifers, the upper is phreatic while the others are confined or partially confined towards the sea. The aquifer has 3-D lithological heterogeneity both at a macro and micro scale level (Ronen et al. 2000). To incorporate into the model the geological structure, 5 available hydrogeological cross-sections about 2000 m apart were digitized and schematized.

At the study area the depth of the domain is around 155 m and 75 m at the western and eastern borders, respectively, parallel to the sea shore. The

groundwater level varies from 0 to 1 m above Mean Sea Level (MSL) at the western border and from 12 to 15 m at the eastern border. As a result of pumping, a groundwater depression was developed in a sub-area of the study domain, during the 1950s. The thickness of the unsaturated zone at the simulated NAPL spill location is about 20 m.

Up-scaling

Multiphase simulators are effective tools for the investigation of complex processes operative in aquifers contaminated by volatile organic contaminants like TCE emerging from spills of NAPL. We followed the model of Forsyth et al. (1988, 1989), Slough et al. (1996, 1999) and Unger et al. (1996, 1998), and studied different operation scenarios. For the sake of comparison of observations at different spatial scales and to scale-up model predictions, we rewrite the mathematical model in a nondimensional form.

We will substitute each η_{ij} scalar, vector or tensor quantity with $\bar{\eta}\eta_{ij}^{/}$, where $\bar{\eta}$ and $\eta_{ij}^{/}$ denote, respectively, the characteristic and dimensionless quantities of η_{ij}. Accounting for equilibrium partitioning of components between the phases, linear adsorption of TCE and isothermal conditions, we write (using Einstein's summation rule concerning repetitive indices) respectively, the nondimensional forms of the *mass balance equations* of the *TCE contaminant* the *water* and *air contaminants,* and the *linear momentum balance equation (Darcy's law)* for each l *phase*

$$\begin{aligned}
&\mathrm{Sh}\frac{\partial}{\partial t^{/}}\left(\phi S_l M_l X_{c_m l}+\rho_b \kappa_d M_l X_{c_m l}\delta_{lq}\right)=\nabla^{/}\cdot\left(\mathrm{Pe}^{-1}\phi S_l \mathbf{D}^{/}_{c_m l} M_l \nabla^{/} X_{c_m l}-M_l X_{c_m l}\mathbf{V}_l^{/}\right);\quad l\equiv n,q,g\\
&\mathrm{Sh}\frac{\partial}{\partial t^{/}}\left(\phi S_l M_l X_{wl}\right)=\nabla^{/}\cdot\left(\mathrm{Pe}^{-1}\phi S_l \mathbf{D}^{/}_{wl} M_l \nabla^{/} X_{wl}-M_l X_{wl}\mathbf{V}_l^{/}\right);\quad l\equiv q,g\\
&\mathrm{Sh}\frac{\partial}{\partial t^{/}}\left(\phi S_g M_g X_{ag}\right)=\nabla^{/}\cdot\left(\mathrm{Pe}^{-1}\phi S_g \mathbf{D}^{/}_{ag} M_g \nabla^{/} X_{ag}-M_g X_{ag}\mathbf{V}_g^{/}\right)\\
&\mathbf{V}_l^{/}=-F\,\mathrm{Re}\frac{k_{rl}}{\mu_l^{/}}\mathbf{K}^{/}\left(\mathrm{Eu}\nabla^{/}P_l^{/}+\frac{\rho_l^{/}}{\mathrm{Fr}}\nabla^{/}Z^{/}\right);\quad \forall_l
\end{aligned}\tag{5}$$

In (5), ϕ denotes the porosity, $\rho_b[kg\,m^{-3}]$ denotes the solid matrix mass density, $\kappa_d[m^3\,kg^{-1}]$ denotes the sorption coefficient, δ_{ij} denotes the Kronecker delta function, $\mathbf{D}_{pl}$ denotes the dispersion tensor for the p component in the l phase, defined by

$$\phi S_l \mathbf{D}_{pl} = \left(\phi S_l D_{pl} + \alpha_{lT} |\mathbf{V}_l|\right)\delta_{ij} + \left(\alpha_{lL} + \alpha_{lT}\right)\frac{V_{li}V_{lj}}{|\mathbf{V}_l|}, \quad \forall l \tag{6}$$

where $D_{pl}[m^2 s^{-1}]$ denotes the diffusion coefficient of p in l, and $\alpha_{lT}, \alpha_{lL}[m]$ denote the transverse and longitudinal dispersivities, respectively, in l.

Note that, $q_p[mole\, m^{-3}\, s^{-1}]$, a source/sink mass flux of the p component is not expressed in (5) for the sake of simplicity. By virtue of (5) we note that the phases and components temporal and spatial distribution is also governed by Sh, Pe, $(F\,\mathrm{Re}\,\mathrm{Eu})$ and $(F\,\mathrm{Re}\,\mathrm{Fr}^{-1})$ numbers, where $\mathrm{Sh} \equiv \left[(L/T)/V_l\right]$ denotes the Strouhal number, $\mathrm{Pe} \equiv \left[\left(V/D_p\right)_l L\right]$ denotes the Peclet number, $\mathrm{Re} \equiv \left[(V/(\mu/\rho))_l L\right]$ denotes the Reynolds number, $\mathrm{Eu} \equiv \left[P/(\rho V^2)\right)_l$ denotes the Euler number, $\mathrm{Fr} \equiv \left[(V_l^2/L)g\right)$ denotes the Froud number and $F \equiv \left[K/L^2\right)$. If the scalar numbers Sh, Pe, $(F\,\mathrm{Re}\,\mathrm{Eu})$ and $(F\,\mathrm{Re}\,\mathrm{Fr}^{-1})$ configured at one spatial scale are made equal to their counterpart numbers obtained at a domain ,say, greater in its spatial scale, one can expect similar flow and transport characteristics in both scales.

Next we will provide examples describing migration patterns resulting from the coupled affect between phases and components when subject to a variety of influences.

Implementations and conclusions

Two Dimensional simulations

To study the effect of the different boundary and initial conditions, operation scenarios and geological formation on the migration of the TCE plume, simulations using synthetic data were considered for a 2-D cross section configuration. The layout of the modelling domain.is depicted in Fig. 1. Extending from the domain left boundary are three clay layers with assumed absolute permeability of $K=10^{-14}$ m^2 each. The absolute permeability of sand was prescribed to be $K=3\ 10^{-11}$ m^2.

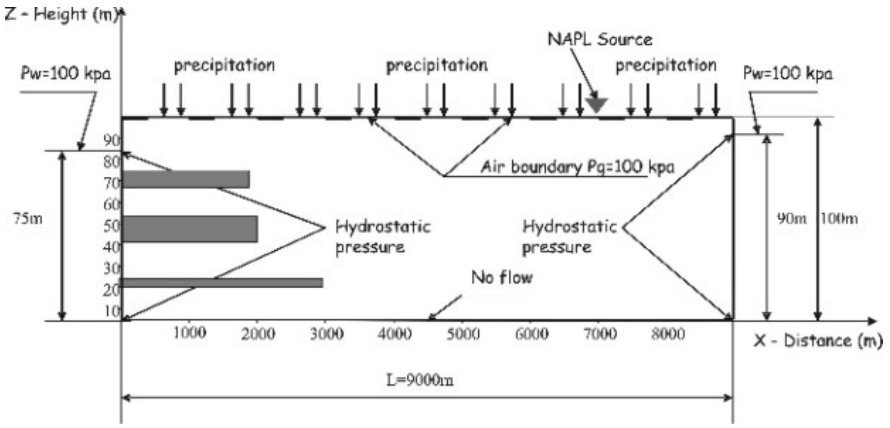

Fig. 1. Computational domain for the two-dimensional, layered, problem, x=0 corresponds to distance of 1500 m from seashore.

The annual replenishment was set to 100 mm for 100 (winter) days. Segments (0% to 80% coverage of the top boundary) of the soil surface were assigned to be impervious to replenishment. Gas was allowed to penetrate through the entire soil surface. Note that components (e.g. TCE) could be displaced outside the domain, as the impervious segments were not assigned a no-flux condition for the fluid phases. The initial aqueous and gaseous regime was determined by transient simulation evolving from a non-stressed aquifer (zero saturation for the non-aqueous phase) and a water table situated at the soil surface. Stabilization of the system took a 10 years period. Forecast was for the next 50 years. NAPL was deployed within one cell of 50 m length ($6950 \le x \le 7000$ m), situated on the surface (Z=100 m). Injection into the soil was constant, over a period of 50 years, with a flux intensity of $q_R = 0.001$ $m^3/m^2/day$. To verify the influence of surface coverage we performed five simulations each with a different percentage (0, 20, 40, 60, and 80%) of surface cover.

Fig. 2 depicts the distribution of phases saturation and TCE mole fraction in the gaseous and aqueous phases for 80%, surface coverage. We note the generation of a thin vertical column of NAPL under the spill. Due to gravity, the NAPL front reached the bottom of the domain in about 10 years. During 40 years it moved downstream (flow direction of the aqueous phase) along the impermeable bottom to a distance of 500 m (460 m for 0% coverage) This displacement was under the influence of the NAPL, saturation dependent, gradient difference between the downstream aqueous pressure and the capillary NAPL pressure. The upstream displacement along the bottom was 40 m (70 m for 0 % coverage).

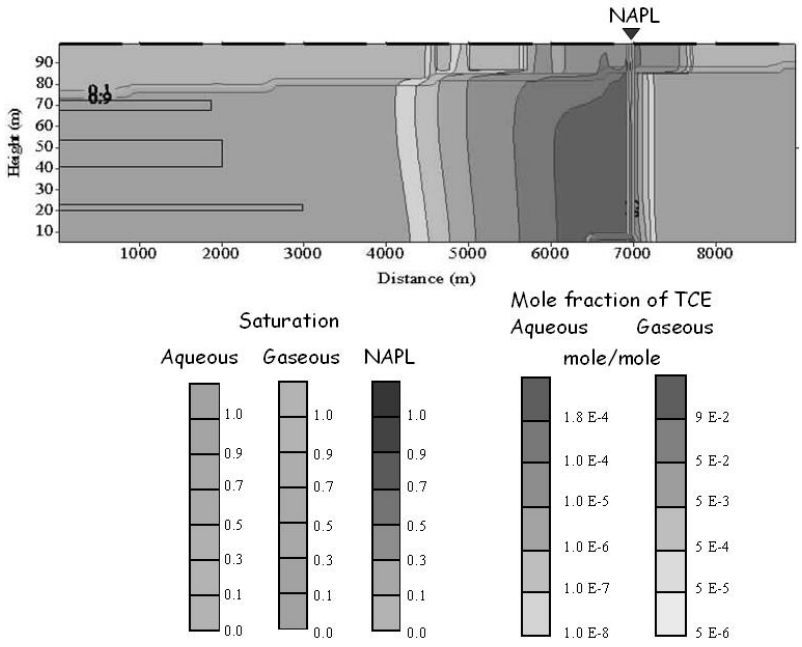

Fig. 2. Saturation and TCE mole fraction in the aqueous and gaseous phases, for the case of 100 mm replenishment over 80% surface coverage in a cyclic pattern, during 100 days per year for 50 years

After 50 years most of the TCE contaminant mass was accumulated in the non-aqueous phase. In the aqueous phase, the concentration profile along the vertical direction became practically uniform. The mole fraction of the TCE changes dramatically crossing along the Saturated–Unsaturated Interface Region. By virtue of Henry's law, TCE has a continuous mole fraction distribution within the aqueous and the gaseous phases yet it is of a lower value in the aqueous phase. Downstream displacement of the maximum TCE concentration in the aqueous phase ($1.8\ 10^{-4}$ mole/mole) was 600 m for the uncovered surface (i.e. 0% coverage), and 900 m for the 80% covered surface. Maximum TCE migration was about 2700-2800 m in groundwater and 2600 m in the unsaturated zone. Upstream TCE displacement in groundwater is similar for both possibilities (0% and 80% coverage). However, in the unsaturated zone the TCE migration distance is to a greater extent for the 80% coverage. Transport of TCE is governed by the phases flow regime. The constant hydrostatic pressure conditions at the right and left boundaries control the hydraulic gradient. However within the domain, the steepness of this gradient is affected by the surface coverage conditions.

The velocity vectors of the aqueous phase are delineated in Fig. 3.A.

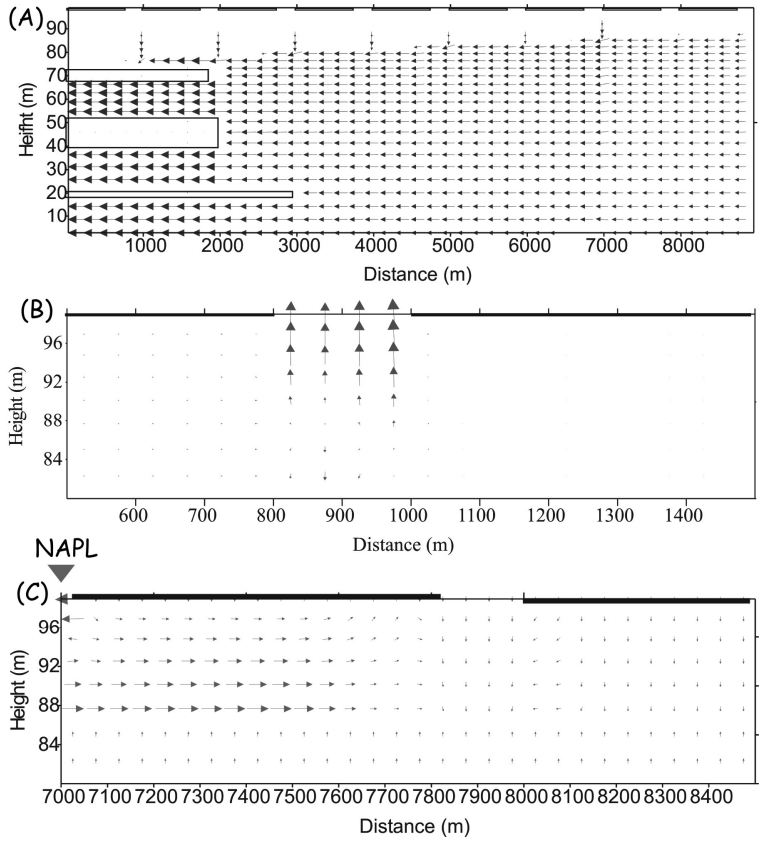

Fig. 3. 100 mm replenishment over 80% surface coverage in a cyclic pattern, during 100 days per year for 50 years. (A) Aqueous velocity pattern. (B) Gaseous flow through an opening during a rainy season. (C) Gaseous flow near the NAPL spill

The typical gaseous flow pattern through the surface uncovered areas is depicted in the snapshot presented in Fig. 3.B. Through these openings infiltration of seasonal rain causes an oscillatory displacement of the aqueous and gaseous phases. The gaseous phase is displaced away from the NAPL phase; its specific flux near the spill is smaller for the uncovered surface case than that of the 80% coverage. At the center of the spill (i.e. along the NAPL column) the NAPL gravity shift causes a vertical gaseous phase velocity also influenced by the gaseous pressure gradient (equal to the gradient of NAPL and capillary pressures**).** As TCE concentration de-

creases away from the NAPL column and since the phases densities are function of TCE concentration, the density gaseous gradient yields its horizontal specific flux (the blowup described in Fig. 3.C) and its vertical outward shift results from the vanishing capillary pressure. Far away from the NAPL column the gaseous velocity is associated with gravity and there are no density driven effects (density is constant as TCE vanishes) and it is diminished at the gaseous-aqueous interface, as its permeability there is zero.

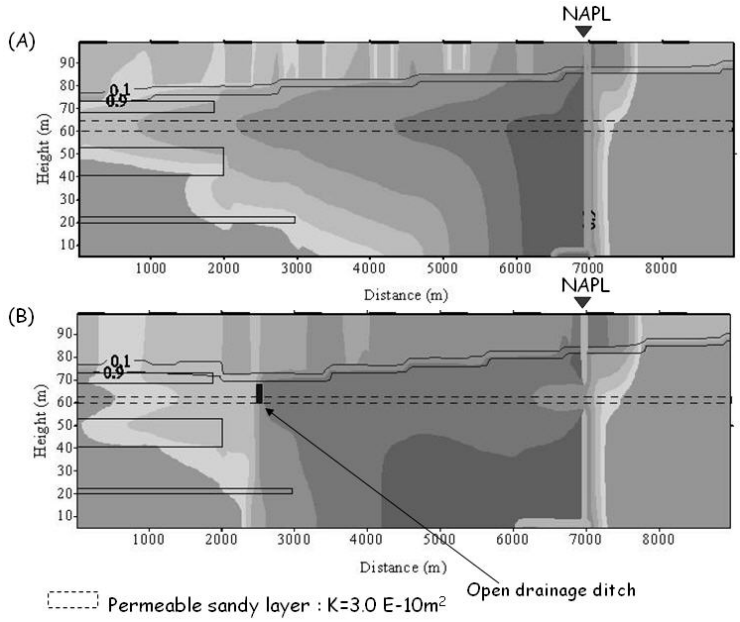

Fig. 4. 100 mm replenishment during 100 days per year over 60% surface coverage in a cyclic pattern, with a preferential flow path. (A) TCE plumes after 50 years. (B) Remediation, due to drainage through an open ditch, for additional 30 years.

To investigate the roll of a preferential flow path, we added a layer with absolute permeability ($K=3\ 10^{-10}\ m^2$) higher than that of the domain. Conditions and replenishment (100 mm per 100 days of each year, over 60% coverage in a cyclic pattern of the soil surface), were as before. Fig. 4.A depicts the extent of TCE migration, centered at the preferential flow path, after a 50 years period.

After the 50 years period of contamination we placed within the preferential flow path an open ditch; Fig. 4.B. describes the extent of the remediation due to the drainage through the ditch. The aqueous flow is augmented at the surroundings of the low permeable layers (Fig. 3.A). This flow pattern forces the amplification of TCE advection, its penetration into the layers due to the dispersion flux and a sideway concentration kink due to the eddy action adjacent to the layers corners (Fig. 4.B).

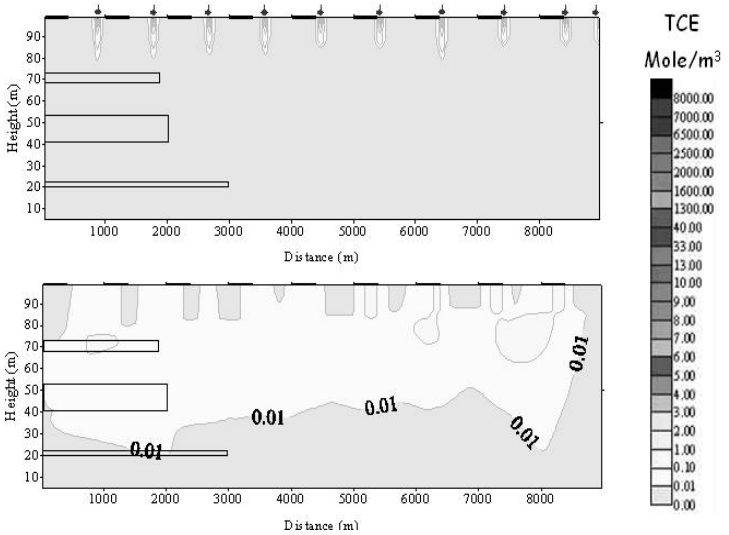

Fig. 5. 100 mm replenishment during 100 days per year, over 40 % surface coverage in a cyclic pattern. (A) Distribution of TCE due to spills lasting 100 days. (B) Distribution of TCE after 50 years.

We now deployed spills for a short duration (100 days), to mimic the notion that there are NAPL residuals in the soil matrix. This can also represent an accidental spill from different sources. The NAPL sources were spread over 10 different locations, uniformly distributed along the soil surface. The previous injection intensity was divided over the 10 locations. Fig. 5.A describes the deployment of the NAPL source for a period of 100 days. Each injection occupied one grid element (50 m), initial and boundary conditions were as for the previous examples, the intensity and distribution of replenishment were as prescribed for the previous example**.** During the first 100 days (Fig. 5.A)**,** the NAPL occupied an extent of 1 to 3 grid elements (2 m to 6.5 m) under the injection point, which practically, because of the small mass amount, enabled us to consider TCE concentration in [mass/volume] units**.** Saturation of NAPL was less then 0.08, there-

fore as the residual NAPL saturation is 0.05 (for which its relative permeability is zero) we conclude that residual NAPL remains adhered to the soil matrix in the unsaturated zone**.** It is evident (Fig. 5.B) that in contrast to the high TCE concentration during the first 100 days, after 10 years TCE was significantly dissolved.

We note (Fig. 5.B) that the neighboring TCE spills joined into a continuous plume (concentration higher than 0.01 mole/m^3), disabling the detection (practically after 10 years) of the individual spill sources. The pronounced aqueous specific flux in between the layers (Fig. 3.A) yields an advective flushing of TCE surrounding the layers; yet (Fig. 5.B) due to the intense dispersion flux at that vicinity, a residual of higher TCE concentration was trapped inside one of the low permeability layers.

Three Dimensional simulations of the study area

The 5 available hydrogeological cross-sections were schematized delineating three main clay layers that divide the main aquifer into 4 sub-aquifers. Interpolation between the cross sections, on the basis of 10 vertical profiles for each cross section enabled an approximate 3-D stratigraphic model of lithological properties and cross-section images anywhere within the investigated domain. A 3-D finite-elements non-uniform mesh (57, 58 and 20 nodes in the x, y and z-directions, respectively), refined at the location of the NAPL source and with vertical variation between 4 to 8 m (depending on the aquifer thickness) was constructed on the basis of the stratigraphic model (Fig. 6).

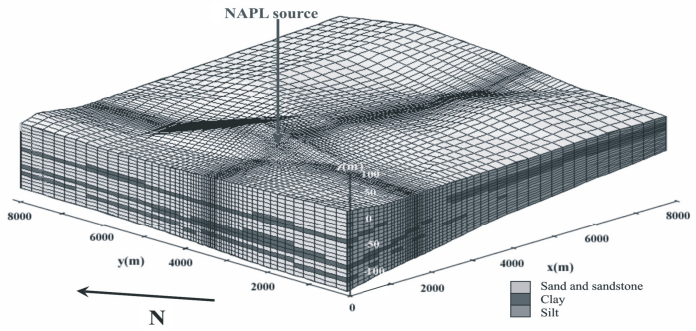

Fig. 6. The modeling domain with the Finite-Element mesh (66,120 nodes)

Available data concerning the location of 106 wells, their pumping rate during the years 1924 to 2000, was gathered into 20 cluster wells (CW) us-

ing a partitioning method (Kaufman and Rousseeuw 1990). The CW distribution and the boundary conditions in the modeling domain are described in Fig. 7. Based on results of sensitivity analysis, we chose the permeability of sand and sandstone as the parameter which was found to be mostly affecting groundwater levels and calibrated the flow model. The comparison between observed and simulated groundwater levels for the year 1980, is presented in Fig. 8. In reality, the actual total amount of NAPL, the size of the discharge area, the discharge intensity and discharge continuity are not known. Taking this into account, we considered 3 different rates of NAPL discharge: 1, 0.2 and 0.02 mm/day, and simulated the multiphase flow and TCE transport during the period 1950 to 2000. In our simulations we assumed that NAPL phase consists of TCE only. For all three cases the aerial extent of the TCE plumes were found to be mimicking the characteristics of the observed TCE plume, but with different distribution patterns. The distribution of TCE concentration in the unsaturated and saturated zones expressed in mole of TCE per mole of aqueous phase is delineated in Fig. 9. Because of the high density of the NAPL phase, its migration through the unsaturated and saturated zones is gravity-driven, and its general displacement is influenced by the hydraulic conductivity, and slope of the different layers. In the unsaturated zone, the NAPL front migrates mainly downwards with an average velocity that decreases upon entering the saturated zone and further attenuates when it reaches the clay layer. Dissolution and volatilization of the NAPL takes place during its movement causing the TCE to be transferred to the aqueous and gaseous phases. Lateral TCE transport through the unsaturated zone occurs mainly in the gaseous phase as the NAPL source is situated within the area covered by an upper impervious boundary (e.g., pavement; Fig. 7). To the west, east and south directions, the velocity of the gaseous phase is higher than groundwater velocity; therefore, secondary contamination of groundwater by TCE dissolving from the gaseous phase is evident.

To the north, groundwater velocity exceeds the velocity of the gaseous phase; therefore, secondary contamination of the unsaturated zone occurs by volatilization of TCE from groundwater far away from the NAPL source (Fig. 8). The transport of TCE in the saturated zone is dominated by advection of groundwater flow, which is directed to the north-east, towards a local groundwater depression. However, the maximum migration of the TCE plume to the south was predicted in the upper part of the aquifer as a result of secondary groundwater contamination. Less intensive NAPL discharge yields less penetration depth, yet migration of TCE in the gaseous phase in the unsaturated zone is similar to the harshest discharge. Additional scenario was simulated for a case when the soil surface was not covered.

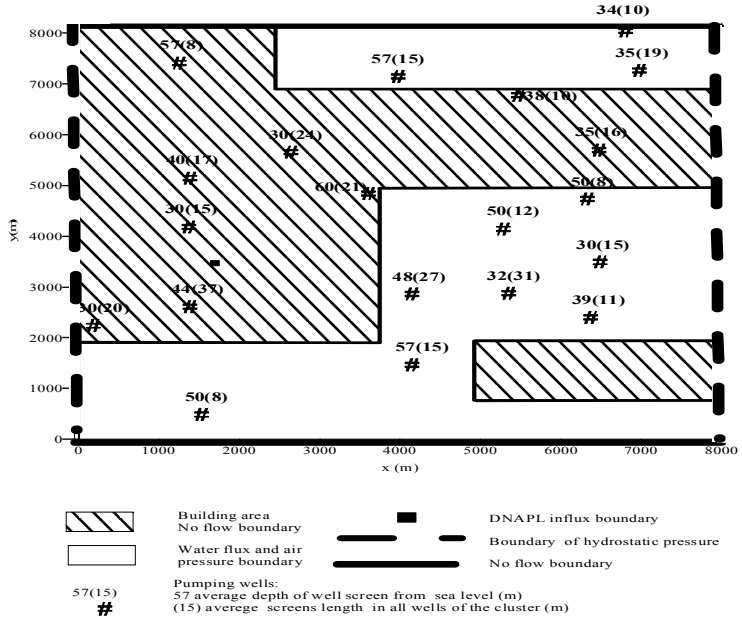

Fig. 7. Schematic representation of boundary conditions in the modeling domain

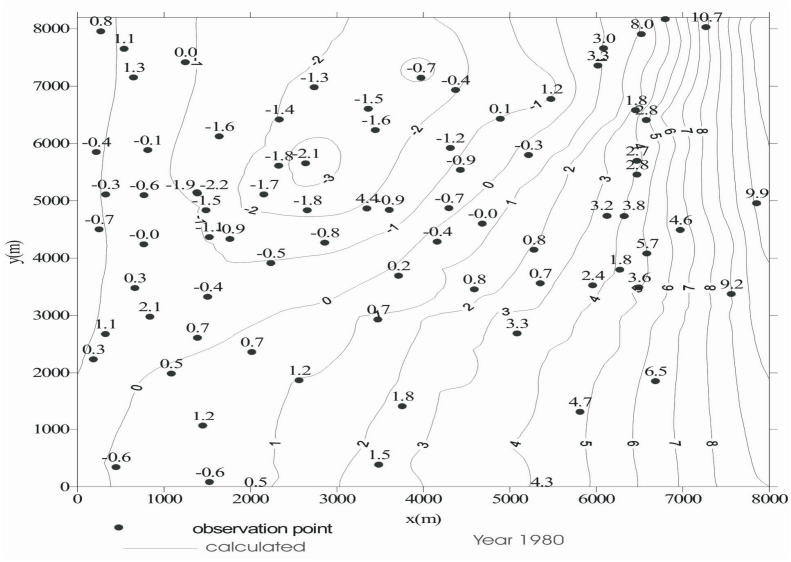

Fig. 8. Comparison between observed (numbers above observation points) and simulated (lines) groundwater levels for the year 1980

Obtained results indicate a significant decrease in the lateral spread of TCE through the unsaturated zone as compared to the case where part of the surface was covered. This is accounted by the fact that the gaseous phase can exit to the atmosphere which also decreases the migration of TCE in groundwater.

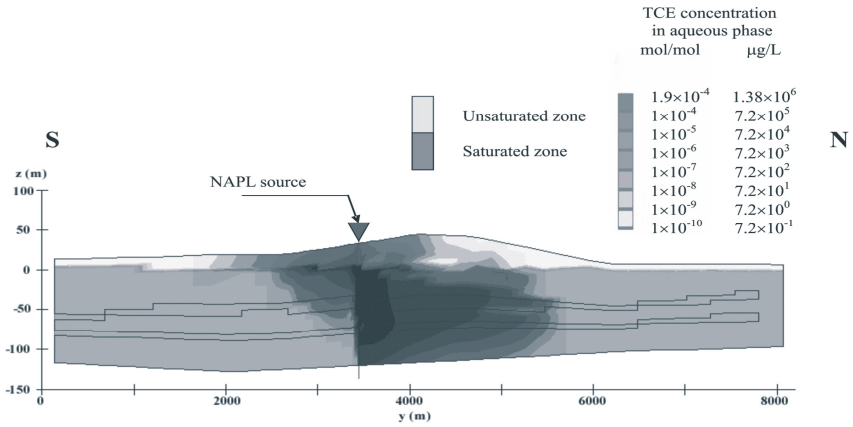

Fig. 9. TCE plumes through a South-North cross-section for the year 2000, subject to the harshest, simulated, NAPL discharge (1 mm/day)

References

Forsyth PA, Unger AJA, Sudicky EA (1998) Nonlinear iteration methods for non-equilibrium multiphase subsurface flow. Adv. Water Resour., on of LNAPL-contaminated aquifers, J Cont Hydrology, 31, pp 57-81

Kaufman L, Rousseeuw PJ (1990) Finding Groups in Data: An Introduction to Cluster Analysis. Wiley, New York

Ronen D, Scher H, Blunt M (2000) Field observations of a capillary fringe before and after a rainy season. Journal of Contaminant Hydrology, Vol. 44, pp 103-118

Slough KJ, Suddicky EA, Forsyth PA (1996) Grid refinement for modeling multi-phase flow in discretely fractured porous media. Adv Water Resour, 23, pp 261-269

Slough KJ, Suddicky EA, Forsyth PA (1999) Numerical simulation of multiphase flow and phase partitioning in discretely fractured geologic media. J Cont Hydrology, 40, pp 107-136

Unger AJA, Forsyth PA, Sudicky EA (1996) Variable spatial and temporal weighting schemes for use in multi-phase compositional problems", Adv Water Resour, Vol. 19, No. 1, pp 1-27

Unger AJA, Forsyth PA, Sudicky EA (1998) Influence of alternative dissolution models and subsurface heterogeneity on DNAPL disappearance times. J Cont Hydrology, 30, pp 217-242